

# Multiple Andreev Reflections in a Carbon Nanotube Quantum Dot

M. R. Buitelaar,<sup>\*</sup> W. Belzig, T. Nussbaumer, B. Babić, C. Bruder, and C. Schönenberger<sup>†</sup>

*Institut für Physik, Universität Basel,  
Klingelbergstrasse 82, CH-4056 Basel, Switzerland*

(Dated: April 9, 2003)

## Abstract

We report resonant multiple Andreev reflections in a multiwall carbon nanotube quantum dot coupled to superconducting leads. The position and magnitude of the subharmonic gap structure is found to depend strongly on the level positions of the single-electron states which are adjusted with a gate electrode. We discuss a theoretical model of the device and compare the calculated differential conductance with the experimental data.

PACS numbers: 74.78.Na,74.45.+c,73.63.Kv,73.21.La,73.23.Hk,73.63.Fg

Keywords: Andreev reflection, quantum dots, carbon nanotubes, electric transport

---

<sup>\*</sup>Present address : Cavendish Laboratory, Cambridge, UK

<sup>†</sup>Electronic address: [Christian.Schoenenberger@unibas.ch](mailto:Christian.Schoenenberger@unibas.ch)

The electronic transport properties of quantum dots coupled to metallic leads have been the object of extensive theoretical and experimental study [1]. When weakly coupled to its leads, the low-temperature transport characteristics are dominated by size and charge quantization effects, parameterized by the single-electron level spacing  $\Delta E$  and the single-electron charging energy  $U_C$ . When the coupling of the quantum dot to the source and drain electrodes is increased, higher-order tunneling processes such as the Kondo effect become important [2]. New effects are expected when the leads coupled to the quantum dot are superconductors. In that case electron transport at small bias voltages is mediated by multiple Andreev reflection (MAR) [3, 4]. Unlike conventional S-N-S devices, however, the MAR structure is now expected [5, 6] to strongly depend on the level positions of the single-electron states of the quantum dot which can be tuned with a gate electrode. The influence of Coulomb and Kondo correlations have been addressed theoretically in Refs. [7].

Because MAR is suppressed rapidly for low-transparency junctions, its observation requires a relatively strong coupling between the leads and quantum dot. Even more so as on-site Coulomb repulsion, which is common to weakly coupled dots, is expected to reduce Andreev processes even further. A quantum dot very weakly coupled to superconducting leads has been studied experimentally by Ralph *et al.* [8]. In this case the transport characteristics were indeed dominated by charging effects and MAR was completely suppressed.

The coupling to the leads, expressed in the life-time broadening  $\Gamma$  of the levels of the quantum dot, should be compared to the superconducting gap energy  $\Delta$ . Favourable for the observation of MAR in a quantum dot are coupling strengths of order  $\Gamma \sim \Delta$  and a small charging energy  $U_C < \Delta$ . Together with the restriction that  $\Gamma < \Delta E$  (for any quantum dot) this leads to the approximate condition  $U_C \lesssim \Gamma \lesssim \Delta E$ . For most quantum dots typically the opposite is true and  $\Delta E \ll U_C$ . It has recently been shown [9] however, that well-coupled multiwall carbon nanotube (MWNT) quantum dots can have favourable ratio's of  $\Delta E/U_C \sim 2$  and  $U_C$  can be as small as 0.4 meV, comparable to the energy gap  $2\Delta$  of a conventional superconductor like Al.

Here we report on the experimental study of resonant MAR in a MWNT quantum dot. The superconducting leads to the MWNT consist of an Au/Al bilayer (45/135 nm). Before investigating the system in the superconducting state, the sample is first characterized in the normal state by applying a small magnetic field. From these measurements relevant parameters such as  $\Delta E$ ,  $U_C$ , and  $\Gamma$  are obtained. We then discuss a theoretical model

that describes the differential conductance of an individual level in a quantum dot coupled to superconducting electrodes. In the final part of the paper we compare the calculated differential conductance with the experimental data.

Figure 1 shows a greyscale representation of the differential conductance  $dI/dV_{sd}$  versus source-drain ( $V_{sd}$ ) and gate voltage ( $V_g$ ) at  $T = 50$  mK when the contacts are driven normal by a small magnetic field. The dotted white lines outline the onset of first-order tunneling and appear when a discrete energy level of the quantum dot is at resonance with the electrochemical potential of one of the leads. From these and other electron states measured for this sample (about 20 in total), we obtain an average single-electron level spacing  $\Delta E \sim 0.6$  meV and a charging energy  $U_C \sim 0.4$  meV. Since  $U_C = e^2/C_\Sigma$  this yields  $C_\Sigma = 400$  aF for the total capacitance which is the sum of the gate capacitance ( $C_g$ ) and the contact capacitances  $C_s$  (source) and  $C_d$  (drain). From the data of Fig. 1a we obtain  $C_g/C_\Sigma = 0.0036$ , and  $C_s/C_d = 0.45$ . The lifetime broadening  $\Gamma$  is obtained from the width of the single-electron peaks at finite source-drain voltage (taking the background conductance into account) and is found to be  $\Gamma \sim 0.35$  meV.

The high-conductance ridge around  $V_{sd} = 0$  mV in Fig. 1a is a manifestation of the spin-1/2 Kondo effect occurring when the number of electrons on the dot is odd. As a result, the Coulomb valley in the conductance has disappeared in this region of  $V_g$  and at 50 mK, which is the base temperature of our dilution refrigerator, only a single peak remains, see Fig. 1b. This is known as the unitary limit of conductance. The appearance of the Kondo effect is an indication that the coupling to the leads is relatively strong. We will not discuss the Kondo effect here, and instead refer to Ref. [10].

When the magnetic field is switched off the leads become superconducting. To calculate the expected differential conductance in the superconducting state of the leads we have used the non-equilibrium Green-function technique [11]. We model the quantum dot as a series of spin-degenerate resonant levels coupled to superconducting electrodes, which are assumed to have a BCS spectral density. Note, that neither electron-electron interaction (Coulomb blockade) nor exchange correlations (Kondo effect) are accounted for in the model, which may, therefore, not explain all details of the actual measurements. However, the interplay between MAR and resonant scattering already leads to strongly nonlinear IV-characteristics and reproduces some of the key features of the data. The details of the model calculation will be presented elsewhere [12]. The main parameters entering the calculation are the two

tunneling rates  $\Gamma_{s(d)} = 2\pi|t_{s(d)}|^2 N_0$ , related to microscopic tunneling amplitudes  $t_{s(d)}$  via the density of states  $N_0$  of the source (drain) contact. In the model we account for the gate voltage by a shift of the level, which can be adjusted according to the experimentally observed Coulomb diamonds, see Fig. 1.

The discrete nature of the single-electron states is most pronounced when  $\Gamma$  is small. Therefore, before presenting the model calculation that directly compares to the experimental data, we first discuss the transport characteristics of a single spin-degenerate level with a relatively weak and symmetric coupling to the superconducting leads along the lines of Refs. [5, 6]. The total tunneling rate  $\Gamma \equiv \Gamma_s + \Gamma_d$  is set to  $\Delta$ . Figure 2 shows the corresponding greyscale representation of the calculated differential conductance  $dI/dV_{sd}$  versus  $\varphi_g := eV_g C_g / C_\Sigma$  and  $eV_{sd}$ . The peak structure in  $dI/dV_{sd}$  at  $V_{sd} < 2\Delta/e$  is the result of MAR. In general, Andreev channels become available for transport at voltages  $V_{sd} = 2\Delta/ne$ , where  $n$  is an integer number. These positions are indicated by the horizontal dashed black lines in Fig. 2a. The appearance and magnitude of the MAR peaks, however, is strongly dependent on the position of the resonant level in the quantum dot with respect to the Fermi energy of the leads. Only those MAR trajectories that connect the resonant level to the leads' BCS spectral densities give a significant contribution to the current. Consider, for example, the position marked by  $C$  in Fig. 2a, which corresponds to the schematics of Fig. 2c and indicates the position  $(\varphi_g, eV_{sd}) = (0, 2\Delta/3)$ . The corresponding second-order Andreev trajectory connects the gap edges of the source and drain electrodes and includes the resonant level which is situated exactly in between the respective Fermi energies. This results in the large peak in  $dI/dV_{sd}$  seen in Fig. 2b.

A similar peak is absent at  $(\varphi_g, eV_{sd}) = (0, \Delta)$ , corresponding to point  $D$  in Fig. 2a. At this voltage, first-order Andreev reflection becomes possible. The corresponding trajectories (see Fig. 2d), however, do not directly connect the resonant level to the leads spectral densities, and therefore do not significantly contribute to the current. Only when the gate voltage is adjusted to align the level with the Fermi energy of one of the leads (indicated by the arrows in Fig. 2a) a peak in  $dI/dV_{sd}$  is observed. It can be shown (for symmetric junctions) that the subharmonic gap structure at  $V_g = 0$  is suppressed for all voltages  $V_{sd} = 2\Delta/ne$  with  $n = \text{even}$  [5, 6]. When  $V_{sd}$  is increased beyond  $\Delta/e$ , peaks are observed either when the level stays aligned with the electrochemical potential of the leads (red dashed lines:  $\varphi_g = \pm eV_{sd}/2$ ) or when the level follows the gap edges as an initial or final state of

an Andreev process (blue dash-dotted lines:  $\varphi_g = \pm(\Delta - eV_{sd}/2)$  or  $\varphi_g = \pm(\Delta - 3eV_{sd}/2)$ ).

We now turn to the actual measurements of the differential conductance when the leads are in the superconducting state. Figure 3 shows a greyscale representation of the measured  $dI/dV_{sd}$  versus  $V_{sd}$  and  $V_g$  at  $B = 0$  mT for the same single-electron state of Fig. 1. A number of differences between the normal state (Fig. 1) and superconducting state (Fig. 3) can be observed. The horizontal high-conductance lines at  $V_{sd} = \pm 0.2$  mV in Fig. 3, for example, are attributed to the onset of quasi-particle tunneling when  $V_{sd} = 2\Delta/e$ . The subgap structure at  $V_{sd} < 2\Delta/e$  (i.e. below 0.2 mV) is attributed to MAR. As anticipated, the magnitude and the position (dashed white lines) of MAR peaks depend on  $V_g$ . To allow for comparison with theory, the adjustable parameters of the model are set to the values obtained from the measurement of Fig. 1. The most important parameter is the coupling between the electrodes and the dot which turns out to be  $\Gamma \sim 3.5 \Delta$ . The voltage division between the two tunnel barriers separating the quantum dot from the leads is  $C_s/C_d = 0.45$ . The individual tunneling rates are not exactly known but are not expected to show a strong asymmetry [13]. The neighboring single-electron states, separated by  $\Delta E \sim 6.5\Delta$ , are included in the calculation. The finite temperature of the experiment is taken into account and set to  $T = 0.1 \Delta$ .

The resulting calculated greyscale representation of the differential conductance is shown in Fig. 4. The overall appearance clearly resembles the measured data of Fig. 3. For example, both the model and the measured data show a large peak in  $dI/dV_{sd}$  around  $V_{sd} = 0$  mV when the electron state is at resonance with the electrochemical potential of the leads (i.e. at  $V_g = 0$ ). When the level is moved away from this position, the linear-response conductance rapidly decays to values below its normal-state value. In contrast, the differential conductance peak at  $V_{sd} = 2\Delta/e$  shows the opposite behavior (both in the model as in the experiment). At  $V_g = 0$ , this peak is much less pronounced than at lower values of  $V_g$ . This can also be seen in the  $dI/dV_{sd}$  line traces of Fig. 3b-c and Fig. 4b-c (solid curves). These observations are similar to conventional S-N-S structures, such as atomic-sized break junctions [14]: for large transparencies of the junction a peak is observed at  $V_{sd} = 0$  but no structure at  $2\Delta$  while for small transparencies a gap is observed around  $V_{sd} = 0$  and a large peak at  $2\Delta$  marks the onset of quasi-particle tunneling. For these systems, the transparency depends on the atomic arrangement of the junction, here the effective transparency can be tuned by moving the level position of a single-electron state with a gate electrode. The

effective transparency is large if the level is aligned with the Fermi levels of the leads (on resonance) and it is small otherwise (off resonance).

The subharmonic gap structure is clearly visible in the measured data of Fig. 3 and has a similar gate-voltage dependence as in the model calculation of Fig. 4. However, there are several differences. The most dramatic one is the pronounced peak at  $(V_g, V_{sd}) = (0, \Delta/e)$  in the measurement (Fig. 3c). Because this position corresponds to an even MAR cycle it should be absent based on our previous consideration (see Fig. 2d).

Let us compare theory and experiment by focussing onto the  $dI/dV_{sd}$  lines traces shown in Fig. 3b-c and Fig. 4b-c (solid curves). In panels b) the dot level is off resonance, while it is on resonance in panels c). For the former case, experiment and theory agree fairly well. The differences in MAR structure between model and experiment are much more pronounced at the resonance position. Whereas the experiment (Fig. 3c) reveals pronounced peaks at  $\Delta/2$ ,  $\Delta$  and  $2\Delta$ , the calculated  $dI/dV_{sd}$  (Fig. 4c, solid) reveals fine structure for small  $V_{sd}$  and pronounced peaks at  $2\Delta/3$  and  $2\Delta$ . According to our previous discussion  $dI/dV_{sd}$  should indeed show a pronounced peak at  $V_{sd} = 2\Delta/3e$ , if the dot level is centered in the middle, i.e. for  $\varphi_g = 0$  at point C in Fig. 2a and Fig. 2c. It rather appears in the experiment that, contrary to expectations, the subgap feature at  $2\Delta/3$  is missing, while the ‘forbidden’ at  $\Delta$  is present. Such behavior would only be expected for very asymmetric junctions having  $C_s/C_d \ll 1$  [15], which is not the case in the present work.

There are different imaginable scenarios that may account for the observed  $\Delta$  peak and the lack of fine structure around  $V_{sd} = 0$  mV in the data of Fig. 3c. Inelastic scattering processes inside the dot, for example, would broaden and obscure higher-order MAR features. Other possible reasons may be found in a broadened BCS spectral density (the superconductor consists of a bilayer of Au/Al [16]) or a suppression of higher-order MAR due to the on-site Coulomb repulsion.

In a phenomenological approach, we may try to account for the additional broadening by manually introducing larger bare couplings  $\Gamma_{s,d}$ . Many curves with varying parameters were calculated of which a representative set is displayed in Fig. 4b-c (dashed curves) corresponding to relatively large dot-electrode couplings of  $\Gamma_s = 2.5 \Delta$  and  $\Gamma_d = 3.5 \Delta$ . For the off-resonance position (Fig. 4b) the main effect of the larger  $\Gamma$  is the increased magnitude of  $dI/dV_{sd}$ . In contrast, the MAR structures significantly changes for the resonance position (Fig. 4c). Remarkably, at large coupling  $\Gamma$ , peaks now appear at  $2\Delta$ ,  $\Delta$  and  $\Delta/2$ . These

peaks do not originate from the resonant level, but from the two neighboring ones which are off resonance (the dot levels are spaced by  $\Delta E \approx 6.5 \Delta$ ). Though the agreement is now reasonable, there is one remaining problem. We were unable to reproduce the relative peak height between the  $2\Delta$  and  $\Delta$  peaks. Using any reasonable set of parameters, the  $2\Delta$  peaks is always larger than the  $\Delta$  peak in the model, while it is the opposite in the experiment. We emphasize that the model does not take into account interaction and correlations. Since a Kondo resonance is observed in the normal state, which need not be suppressed in the superconducting state [10], this may be the origin of the discrepancy. The Kondo resonance changes the spectral density in the leads by adding spectral weight to the center of the gap and removing spectral weight from the gap edges. The former tends to enhance the  $\Delta$  peak, while the latter tends to suppress the  $2\Delta$  one. This explanation is attractive, but more work both in theory and experiment is needed to substantiate it.

In conclusion, we have investigated the non-linear conductance characteristics of a quantum dot coupled to superconducting electrodes. We find a strong dependence of the MAR structure on the level position of the single-electron states. The experimental data is compared with a theoretical model, assuming a BCS density-of-states in the electrodes and an interaction-free dot. Reasonable agreement is possible, if the tunneling coupling to the leads is enhanced by a factor  $\sim 2$  in the model as compared to the experimental value. There are additional subtle differences which point to the importance of interaction and exchange correlations.

### Acknowledgments

We acknowledge contributions by H. Scharf and M. Iqbal. We thank L. Forró for the MWNT material and J. Gobrecht for providing the oxidized Si substrates. This work has been supported by the Swiss NFS, BBW, and the NCCR on Nanoscience.

- 
- [1] L.P. Kouwenhoven *et al.*, in *Mesoscopic Electron Transport*, edited by L.L. Sohn, L.P. Kouwenhoven, and G. Schön (Kluwer, Dordrecht, The Netherlands, 1997).
  - [2] L. Kouwenhoven and L. Glazman, *Phys. World* **14**, No.1, 33-38 (2001).
  - [3] A.F. Andreev, *Sov. Phys. JETP* **19**, 1228 (1964).

- [4] M. Octavio, M. Tinkham, G.E. Blonder, and T.M. Klapwijk, Phys. Rev. B. **27**, 6739 (1983).
- [5] A. Levy Yeyati, J.C. Cuevas, A. López-Dávalos, and A. Martín-Rodero, Phys. Rev. B **55**, R6137 (1997).
- [6] G. Johansson, E.N. Bratus, V.S. Shumeiko, and G. Wendin, Phys. Rev. B **60**, 1382 (1999).
- [7] Y. Avishai, A. Golub, and A.D. Zaikin, Phys. Rev. B **63**, 134515 (2001); Y. Avishai, A. Golub, and A.D. Zaikin, Phys. Rev. B **67**, 041301 (2003).
- [8] D.C. Ralph, C.T. Black, and M. Tinkham, Phys. Rev. Lett. **74**, 3241 (1995).
- [9] M. R. Buitelaar, A. Bachtold, T. Nussbaumer, M. Iqbal, and C. Schönenberger, Phys. Rev. Lett. **88**, 156801 (2002).
- [10] M. R. Buitelaar, T. Nussbaumer, and C. Schönenberger, Phys. Rev. Lett. **89**, 256801 (2002).
- [11] J. Rammer and H. Smith, Rev. Mod. Phys. **58**, 323 (1986).
- [12] W. Belzig *et al.*, in preparation.
- [13] The saturation of the Kondo resonance of Fig. 1 close to  $2e^2/h$  suggests that the tunneling rates of both junctions are quite similar.
- [14] E. Scheer *et al.*, Phys. Rev. Lett. **78**, 3535 (1997).
- [15] G. Johansson, V.S. Shumeiko, E.N Bratus, and G. Wendin, Physica C **293**, 77 (1997);
- [16] E. Scheer *et al.*, Phys. Rev. Lett. **86**, 284 (2001).

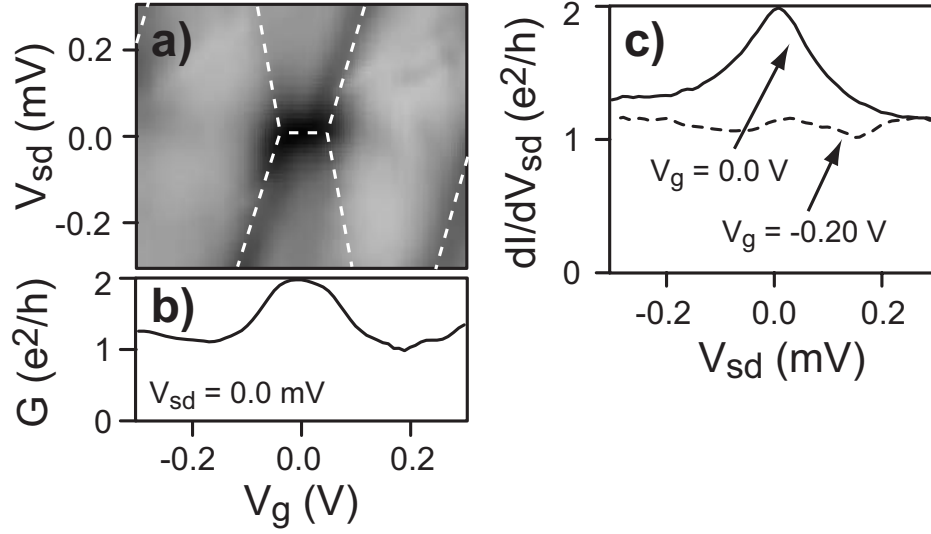


FIG. 1: **(a)** Greyscale representation of the differential conductance as a function of source-drain ( $V_{sd}$ ) and gate voltage ( $V_g$ ) at  $T = 50$  mK and  $B = 26$  mT for a MWNT quantum dot. Here and in the following greyscale plots, the darker a region the higher the differential conductance. The dashed lines outline the onset of first-order tunneling processes. **(b)** Linear-response conductance  $G$  as a function of  $V_g$ . The appearance of a single broad peak is due to the Kondo effect. **(c)** Differential conductance at two different values of  $V_g$ .

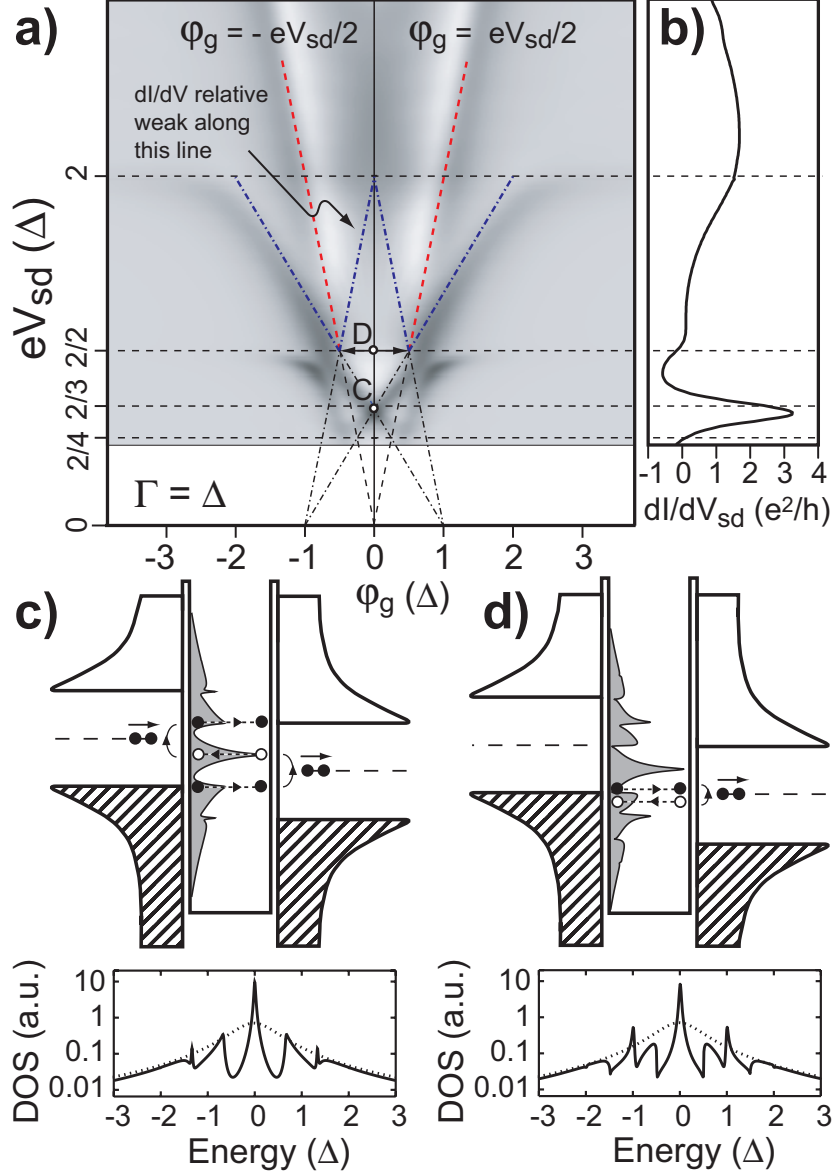


FIG. 2: **(a)** Greyscale representation of the calculated differential conductance as a function of  $V_{sd}$  and level position ( $\varphi_g \propto V_g$ ) for a single-electron level coupled symmetrically to superconducting electrodes. For clarity, the low-energy part  $eV_{sd} \lesssim 2\Delta/4$  has been omitted. The dashed lines indicate resonance positions, as explained in the text. **(b)** Differential conductance at  $\varphi_g = 0$ . Note, that MAR peaks at  $2\Delta/n$  are suppressed for even values of  $n$ . **(c)** Schematics of a single electron state between superconducting source and drain electrodes. The situation shown corresponds to point *C* in panel (a). The spectral density is shown at the bottom. The Lorentzian level broadening in the normal state is replaced by a narrow central resonance accompanied by a series of satellite peaks. **(d)** Same as (c) for point *D* in panel (a).

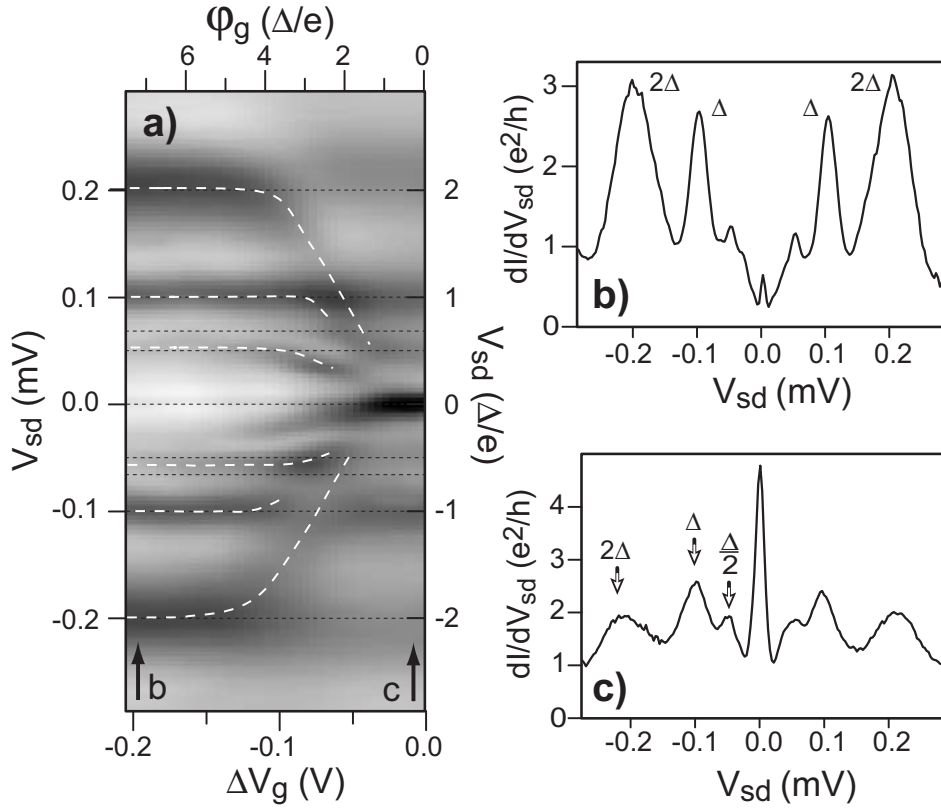


FIG. 3: **(a)** Greyscale representation of the measured differential conductance as a function of  $V_{sd}$  and  $V_g$  at  $T = 50$  mK with the leads in the superconducting state. The gate voltage range corresponds to the left part of Fig. 1a. The dashed white lines emphasize the position of the MAR peaks. **(b-c)** Differential conductance at the positions given in panel (a).

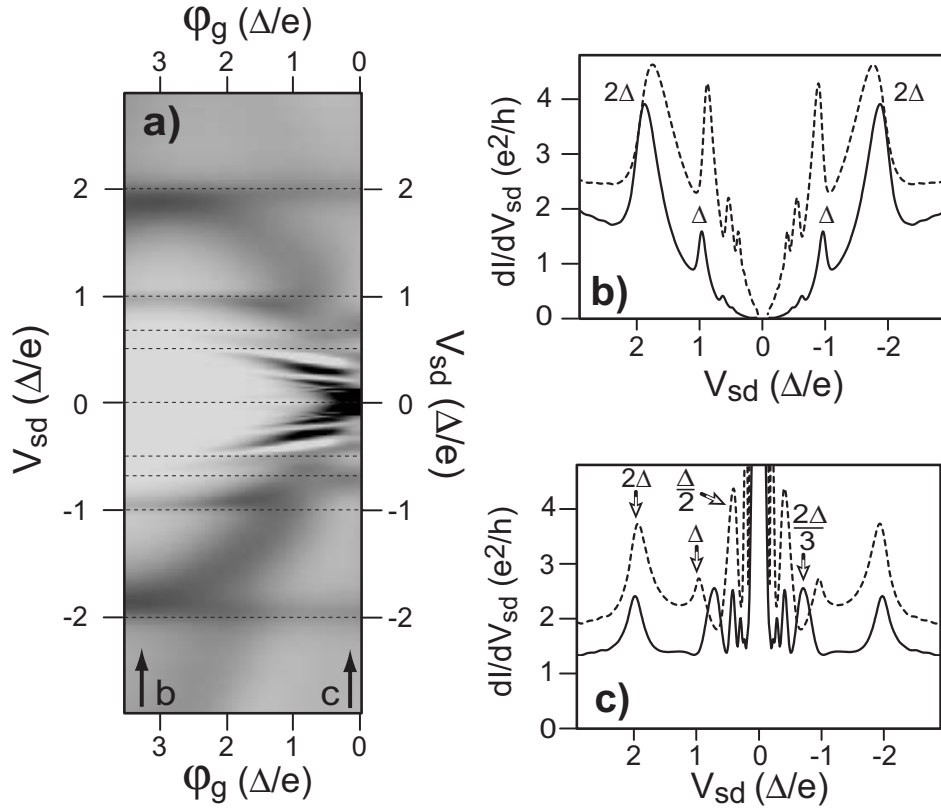


FIG. 4: **(a)** Greyscale representation of the calculated differential conductance as a function of  $V_{sd}$  and level position ( $\phi_g$ ). The different adjustable parameters represent the experimental situation, see text. **(b-c)** Differential conductance at the positions given in panel (a). For the two dashed curves,  $\Gamma$  has been chosen approximately twice as large as the experimental value.